Journal of Hazardous Materials 217–218 (2012) 92–99

Contents lists available at SciVerse ScienceDirect

Journal of Hazardous Materials

journal homepage: www.elsevier.com/locate/jhazmat

High-performance porous spherical or octapod-like single-crystalline $BiVO_4$ photocatalysts for the removal of phenol and methylene blue under visible-light illumination

Haiyan Jiang, Xue Meng, Hongxing Dai*, Jiguang Deng, Yuxi Liu, Lei Zhang, Zhenxuan Zhao, Ruzhen Zhang

Laboratory of Catalysis Chemistry and Nanoscience, Department of Chemistry and Chemical Engineering, College of Environmental and Energy Engineering, Beijing University of Technology, Beijing 100124, China

ARTICLE INFO

Article history:
Received 6 January 2012
Received in revised form 9 February 2012
Accepted 28 February 2012
Available online 6 March 2012

Keywords:
Surfactant-assisted hydrothermal preparation method
Porous bismuth vanadate single-crystallite
Visible-light-driven photocatalyst
Phenol removal
Dye photodegradation

ABSTRACT

Monoclinic $BiVO_4$ single-crystallites with a polyhedral, spherical or porous octapod-like morphology were selectively prepared using the triblock copolymer P123 ($HO(CH_2CH_2O)_{20}(CH_2CH(CH_3)O)_{70}(CH_2CH_2O)_{20}H$)-assisted hydrothermal method with bismuth nitrate and ammonium metavanadate as metal source and various bases as pH adjustor. The $BiVO_4$ materials were well characterized and their photocatalytic activities were evaluated for the removal of methylene blue (MB) and phenol in the presence of a small amount of H_2O_2 under visible-light illumination. It is shown that the pH value of the precursor solution, surfactant, and hydrothermal temperature had an important impact on particle architecture of the $BiVO_4$ product. The introduction of P123 favored the generation of $BiVO_4$ with porous structures. The $BiVO_4$ derived hydrothermally with P123 at pH 3 or 6 possessed good optical absorption performance both in UV- and visible-light regions and hence showed excellent photocatalytic activities for the degradation of MB and phenol. It is concluded that the high visible-light-driven catalytic performance of the porous octapod-like $BiVO_4$ single-crystallites is associated with the higher surface area, porous structure, lower band gap energy, and unique particle morphology. Such porous $BiVO_4$ materials are useful in the solar-light-driven photocatalytic treatment of organic-containing wastewater.

1. Introduction

$BiVO_4$ is an important material utilized in ferroelastics [1], conductors [2], and photocatalysis [3,4]. Its physicochemical properties are intimately associated with the crystalline structure, particle morphology, porous structure, and nano/microstructure. In the past years, $BiVO_4$-based materials have been investigated intensively and extensively due to their potential applications in the photocatalytic treatment of organic-containing wastewater.

Among the three crystalline structures (i.e., tetragonal zircon, monoclinic scheelite, and tetragonal scheelite) of $BiVO_4$, the monoclinic scheelite one exhibits the best photocatalytic activity under visible-light irradiation [3,4]. The crystal phase of $BiVO_4$ is strongly dependent on the preparation method employed. The tetragonal $BiVO_4$ is usually obtained by aqueous precipitation at low temperatures, whereas the monoclinic $BiVO_4$ can be generated via the solid-state reaction [5], hydrothermal treatment [6–11], organometallic decomposition [12,13], and sonochemical routes [14]. Among these methods, the hydrothermal one attracts increasing attention due to its simplicity and effectiveness in generating monoclinically crystallized $BiVO_4$ with regular particle morphologies in an environmentally benign way [6,8,10]. Factors, such as precursor nature and concentration, surfactant, precursor solution pH value, hydrothermal temperature and time as well as subsequent thermal treatment, exert important impacts on the crystal structure and particle morphology of the product. A large number of $BiVO_4$ with different crystal phases and architectures have been reported in the literature. For instance, Xie and coworkers [15] obtained monoclinic $BiVO_4$ with hyperbranched structures by hydrothermally treating the $Bi(NO_3)_3$ and $NaVO_4$ mixture under an acidic condition at 200 °C; Yu and Kudo adopted a hydrothermal process to fabricate monoclinic scheelite $BiVO_4$ particles with polyhedral and rod-like shapes using $Bi(NO_3)_3$ and NH_4VO_3 as metal precursor and urea or ammonia as pH adjusting agent [6]. By employing a simple reflux procedure with $Bi(NO_3)_3$ and NH_4VO_3 as metal source and $NaHCO_3$ as pH adjustor, Wang and coworkers prepared single-crystalline monoclinic $BiVO_4$ microtubes [16]. In another work, Yu and Kudo [8] reported the preparation of $BiVO_4$ nanofibers via a cetyltrimethylammonium bromide (CTAB)-assisted hydrothermal process, in which CTAB played a crucial role

* Corresponding author. Tel.: +86 10 6739 6118; fax: +86 10 6739 1983.
E-mail address: hxdai@bjut.edu.cn (H. Dai).

0304-3894/$ – see front matter © 2012 Elsevier B.V. All rights reserved.
doi:10.1016/j.jhazmat.2012.02.073

in controlling the phase structure and morphology of the product. With CTAB as surfactant and Bi_2O_3 and NH_4VO_3 as metal precursor, Li et al. hydrothermally prepared monoclinic $BiVO_4$ microparticles with cuboid-, square plate-, and flower-like shapes [11]. With the aid of a surfactant (e.g., CTAB, polyvinyl alcohol or polyvinyl pyrrolidone), $BiVO_4$ with rod-, slice-, flower-, and sphere-like morphologies could be obtained using the hydrothermal method with $Bi(NO_3)_3$ and NH_4VO_3 as the starting materials [17].

As an effective visible-light-responsive photocatalyst, $BiVO_4$ is highly required to possess a low band gap energy (favoring the absorption of visible light) and high surface area (facilitating the adsorption of reactant molecules). Up to now, however, only several works relevant to the preparation of high-surface-area porous monoclinic $BiVO_4$ crystals have been reported in the literature. For example, ordered mesoporous monoclinic $BiVO_4$ with a surface area of 59 m^2/g was obtained through a nanocasting pathway with mesoporous silica (KIT-6) as template, and the mesoporous $BiVO_4$ performed well in catalyzing the degradation of methylene blue (MB) under visible-light irradiation [18]; using a hydrothermal method, Zhou et al. generated monoclinic $BiVO_4$ (surface area = 15.6 m^2/g) and observed a high activity for MB degradation under visible-light illumination [19]. Organics (such as phenol and MB) in wastewater originated from chemical industries are toxic, carcinogenic, teratogenic, and refractory in nature. It is highly desirable to develop a "green" and energy-saving strategy to remove these organic pollutants from wastewater. It was found that the B-TiO_2 [20], Bi_2WO_6 [21], and Bi_2MoO_6 [22] materials were photocatalytically active for the treatment of phenol-containing wastewater. Although monoclinic $BiVO_4$ possesses a narrow band gap, it displays a poor photocatalytic activity due to the difficulty in capturing the photoinduced electrons by oxygen [23]. In the presence of H_2O_2 (an electron scavenger), however, an enhancement in photocatalytic performance of $BiVO_4$ could be achieved for the removal of phenol under visible-light illumination [23–25].

Previously, our group investigated the preparation and physicochemical property characterization of a number of porous and/or nano/microstructured materials, such as mesoporous MgO [26] and CaO [27] single-crystallites and three-dimensionally (3D) ordered macroporous γ-Al_2O_3 and $Ce_{1-x}Zr_xO_2$ with mesoporous walls [28], by means of the surfactant (e.g., triblock copolymers poly(ethylene glycol)-poly(propylene glycol)-poly(ethylene glycol) Pluronic P123 ($HO(CH_2CH_2O)_{20}(CH_2CH(CH_3)O)_{70}(CH_2CH_2O)_{20}H$) and F127 ($HO(CH_2CH_2O)_{106}(CH_2CH(CH_3)O)_{70}(CH_2CH_2O)_{106}H$), CTAB or poly(ethylene glycol))-assisted hydrothermal strategies. Recently, we have extended our attention to the selective preparation of visible-light-responsive monoclinic bismuth vanadates with polyhedral, tubular, spherical, rod-like, leaf-like, flower-like, sheet-like, and olive-like morphologies via the hydrothermal or alcoho-hydrothermal routes with water, ethanol or ethylene glycol as solvent and/or dodecylamine, oleylamine, oleic acid or triblock copolymer as surfactant [29–31], in which a morphology-dependent photocatalytic behavior was observed for the photodegradation of organic dyes and phenol. Compared to one of our previous works [31], our present work focuses on the P123-assisted preparation, characterization, and excellent photocatalytic performance of monoclinic $BiVO_4$ single-crystallites with multiple morphologies and/or porous structures for the removal of MB and phenol in the presence of a small amount of H_2O_2 under the visible-light illumination.

2. Experimental

2.1. Catalyst preparation

The $BiVO_4$ photocatalysts with different morphologies were prepared using the hydrothermal method with $Bi(NO_3)_3{\cdot}5H_2O$ and NH_4VO_3 as metal source in the absence and presence of triblock copolymer surfactant P123. The detailed procedures were described in the Supplementary data. For better presentation, we denoted the samples prepared under various conditions as $BiVO_{4-x}$ (x = I, II, III, IV, and V), as shown in Table 1.

2.2. Catalyst characterization

The samples were characterized by means of X-ray diffraction (XRD), thermogravimetric analysis (TGA), differential scanning calorimetric (DSC) analysis, laser Raman spectroscopy, N_2 adsorption–desorption (BET), scanning electron microscopy (SEM), transmission electron microscopy (TEM), selected-area electron diffraction (SAED), and ultraviolet-visible (UV-Vis) diffuse reflectance spectroscopy. The detailed procedures were described in the Supplementary data.

2.3. Photocatalytic performance evaluation

Photocatalytic activities of the samples for the removal of MB or phenol were measured in a quartz reactor (QO250, Beijing Changtuo Sci. & Technol. Co. Ltd.) under visible light irradiation. A 300-W Xe lamp was employed as the light source and an optical cutoff filter was used to only permit the illumination of light with a wavelength of higher than 400 nm. (i) 0.01 g of the $BiVO_4$ or commercial TiO_2 (Degussa P25) sample was suspended in 100 mL of aqueous solution containing MB (initial MB concentration C_0 = 0.01 mmol/L) or (ii) 0.2 g of the $BiVO_4$ or P25 sample and 0.6 mL of H_2O_2 solution (30 wt%) were added to 200 mL of the phenol-containing aqueous solution (initial phenol concentration C_0 = 0.1, 0.2 or 0.4 mmol/L). Before illumination, the mixed solution was ultrasonicated for 0.5 h and magnetically stirred for 3 h in the dark to ensure the establishment of the adsorption–desorption equilibrium. Then the suspension was magnetically stirred and exposed to the visible-light irradiation. The temperature of the reaction solution was kept at ca. 25 °C using flowing cool water. 5 mL of the suspension was

Table 1
Preparation conditions, crystal structures, particle morphologies, BET surface areas, and band gap energies of the as-prepared $BiVO_4$ samples.

Sample code	Surfactant[a]	Alkaline source	pH	Hydrothermal condition[b]	Crystal structure	Particle morphology	Surface area (m^2/g)	Band gap energy (eV)
$BiVO_4$–I	P123	$NH_3{\cdot}H_2O$	3	180 °C, 6 h	Monoclinic	Polyhedral (major), porous octapod-like (minor)	0.7	2.43
$BiVO_4$–II	P123	$NaHCO_3$	6	180 °C, 6 h	Monoclinic	Porous spherical (major), polyhedral (minor)	8.1	2.42
$BiVO_4$–III	P123	$NH_3{\cdot}H_2O$	3	80 °C, 6 h	Monoclinic	Porous octapod-like	11.8	2.38
$BiVO_4$–IV	P123	$NH_3{\cdot}H_2O$	3	100 °C, 6 h	Monoclinic	Porous octapod-like	8.6	2.41
$BiVO_4$–V	–	$NH_3{\cdot}H_2O$	3	180 °C, 6 h	Monoclinic	Hyperbranched	2.0	2.44

[a] The $BiVO_4$ samples were prepared with a Bi/P123 molar ratio of 1:0.034.
[b] After hydrothermal treatments, the obtained solids were calcined at 400 °C for 4 h.

taken out at 15 min intervals for MB photodegradation or 30 min intervals for phenol photodegradation and centrifuged to remove the photocatalyst particles for the analysis of MB or phenol concentration. The concentration of MB or phenol in the solution was monitored by determining the absorbance of the MB or phenol solution at ca. 665 nm for the former or ca. 280 nm for the latter during the photodegradation process on the aforementioned UV-Vis equipment. The ratio (C_t/C_0) of MB or phenol concentrations after reaction for some time (C_t) and at the initial (C_0) was used to evaluate the photocatalytic performance.

3. Results and discussion

3.1. Crystal structure and surface area

Fig. 1 shows the XRD patterns of the as-prepared $BiVO_4$ samples. It can be realized that all of the Bragg diffraction peaks of each sample in the 2θ range of 10–70° could be well indexed, as indicated in Fig. 1(e), to single-phase monoclinic crystal $BiVO_4$ (JCPDS PDF# 83-1700), in good consistency with the results reported by other researchers [6–11,14–17,32–36]. The crystallite sizes of $BiVO_4$–I, $BiVO_4$–II, $BiVO_4$–III, $BiVO_4$–IV, and $BiVO_4$–V estimated from the XRD patterns were 31, 46, 30, 28, and 30 nm, respectively. The small discrepancy in peak intensity is indicative of no significant difference in crystallinity of the five $BiVO_4$ samples. The formation of single-phase monoclinic $BiVO_4$ in each sample implies that the calcination temperature (400 °C) was appropriate. Such a deduction was confirmed by the results of TGA/DSC studies (Fig. S1 of the Supplementary data), in which a weight loss of ca. 1.1 wt% was detected for the $BiVO_4$–3 sample before calcination at 400 °C for 4 h. The weight loss was due to the removal of small amounts of surface adsorbed water and P123 (which could be oxidized below 400 °C) plausibly embedded in the $BiVO_4$ entities because a porous structure of $BiVO_4$ was generated after calcination at 400 °C, as evidenced by its SEM observations below. The laser Raman investigation also confirmed the formation of single-phase monoclinic $BiVO_4$ in each sample (Fig. S2 of the Supplementary data). Therefore, thermally treating the precursors of $BiVO_4$ obtained after the hydrothermal treatment at 400 °C could guarantee the complete removal of the surfactant P123 and adsorbed water.

Table 1 summarizes the preparation conditions and partial physical properties of the $BiVO_4$ samples. There was a big difference in surface area of the five samples. The $BiVO_4$–II, $BiVO_4$–III, and $BiVO_4$–IV samples showed a much higher surface area (8.1 – 11.8 m^2/g) than the $BiVO_4$–I and $BiVO_4$–V ones (0.7 – 2.0 m^2/g), with the $BiVO_4$–III sample possessing the highest surface area (11.8 m^2/g). Such a high surface area of $BiVO_4$–III was due to the formation of a number of pores on the particle surfaces, as confirmed by the SEM observations. Most of the monoclinic $BiVO_4$ materials reported in the literature exhibited low surface areas (<3.0 m^2/g), especially when they were generated after calcination at high temperatures (≥400 °C) [3,4,6,7,35,36].

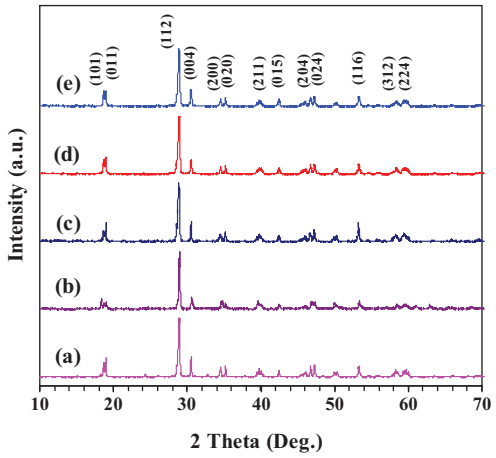

Fig. 1. XRD patterns of the $BiVO_4$–x samples with x = I (a), II (b), III (c), IV (d), and V (e).

3.2. Morphology and formation mechanism

Shown in Fig. 2 are the SEM images of the $BiVO_4$ samples. It can be realized that the morphology of $BiVO_4$ was mainly dependent on the pH value of the precursor solution and the hydrothermal treatment temperature. The microparticles of the $BiVO_4$–I sample were mainly polyhedral in morphology, but a small amount of irregular octapod-like particles with a porous structure was also formed in $BiVO_4$–I. The employment of $NaHCO_3$ for pH value regulation, however, led to the generation of spherical (6–8 μm in diameter) $BiVO_4$ particles with porous surfaces and of a small amount of polyhedral particles. Irregularly spherical $BiVO_4$ submicroparticles were also generated via a homogeneous precipitation route with the aid of *N*,*N*-dimethylacetamide or *N*-methyl-2-pyrrolidone [37]. With P123 as surfactant and $NH_3{\cdot}H_2O$ as pH regulator at a hydrothermal temperature of 80 °C for 6 h, the $BiVO_4$–III particles obtained before and after calcination at 400 °C showed a regular octapod-like morphology; no pores were formed on the octapod-like particle surfaces of the uncalcined $BiVO_4$–III sample (Fig. 2(e) and (f)), but there were a number of pores on the particle surfaces of the calcined $BiVO_4$–III sample (Fig. 2(g) and (h)), which rendered this sample to possess a higher surface area. Such a porous structure was generated due to the oxidative decomposition of surfactant P123 possibly embedded in the $BiVO_4$ entities during the hydrothermal process. With the rise in hydrothermal temperature from 80 to 100 °C, the as-obtained $BiVO_4$–IV sample remained the octapod-like morphology and porous structure (Fig. 2(i) and (j)). A further rise in hydrothermal temperature to 180 °C gave rise to the formation of $BiVO_4$–I that contained a number of polyhedral particles and a small amount of irregular octapod-like particles with porous surfaces. In the absence of P123, however, particles of the obtained $BiVO_4$–V displayed a hyperbranched morphology with a trunk length of 1–3 μm. Such similarly morphological monoclinic $BiVO_4$ materials were also fabricated by other researchers [7,32] who adopted an aqueous process with $Bi(NO_3)_3$ and NH_4VO_3 as metal source. From the above results, one can conclude that the pH value of the precursor solution, surfactant P123, and hydrothermal temperature played a crucial role in governing the morphology and porous structure of the $BiVO_4$ product.

Fig. 3 shows the TEM and high-resolution TEM images as well as the SAED patterns of three typical $BiVO_4$ samples with spherical ($BiVO_4$–II), porous octapod-like ($BiVO_4$–III), and hyperbranched ($BiVO_4$–V) morphologies. The TEM images of the $BiVO_4$–I and $BiVO_4$–IV samples are shown in Fig. S3 of Supplementary data. Due to the thickness of the sample particles, it is difficult to obtain clear high-resolution TEM images of lattice fringes. By checking the high-resolution TEM images carefully, one can estimate the *d* spacings of the (1 1 2) and (1 1 6) crystal planes of the three $BiVO_4$ samples to be ca. 0.31 and 0.18 nm, respectively, not far away from those (0.30817 nm for the (1 1 2) crystal plane and 0.17203 nm for the (1 1 6) crystal plane) of the standard $BiVO_4$ sample (JCPDS PDF# 83-1700). The recording of a number of bright spots aligned linearly (insets of Fig. 3(a, d, and g)) demonstrates the generation of high-quality monoclinic $BiVO_4$ single-crystallites. It is worth pointing out that the most exposed crystal planes of our $BiVO_4$ samples were the (1 1 2) and (1 1 6) planes, but other researchers [15,16,32] obtained monoclinic $BiVO_4$ materials with the most exposed crystal planes of (0 2 0), (0 0 2), (0 1 1), (1 1 4), and/or (2 0 0), a result

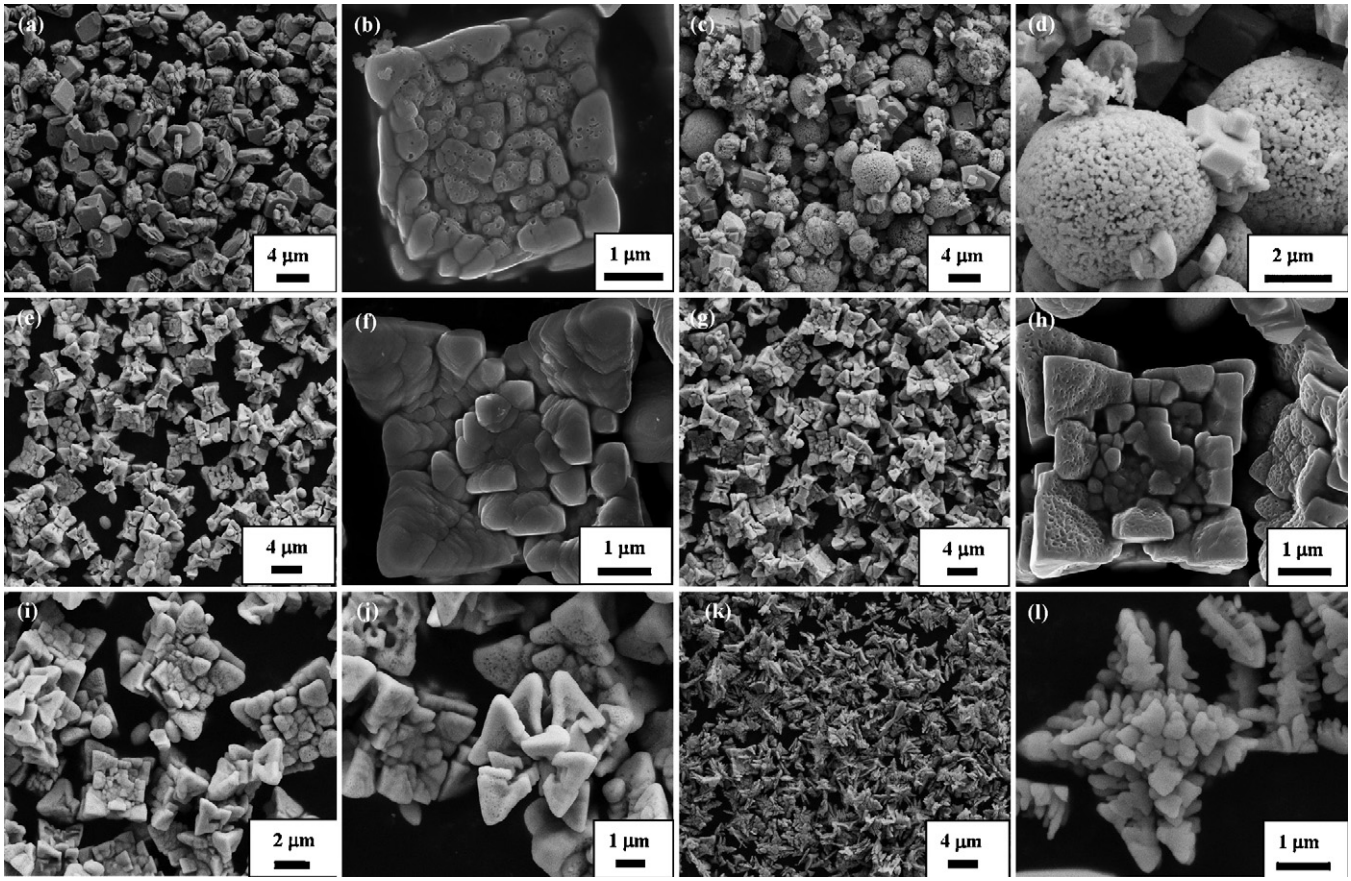

Fig. 2. SEM images of (a, b) $BiVO_4$–I, (c, d) $BiVO_4$–II, (e, f) uncalcined $BiVO_4$–III, (g, h) $BiVO_4$–III, (i, j) $BiVO_4$–IV, and (l, m) $BiVO_4$–V.

probably due to the discrepancies in particle morphology, porous structure, and single-crystallinity derived from various preparation routes.

In the hydrothermal synthesis of a solid material, the nature of surfactant, alkaline source, and metal precursor, pH value of the precursor solution, and hydrothermal temperature and time have great influence on the morphology of the final product [6,15,16,32,38]. The oriented aggregation mechanism [39–44] has been proposed to successfully explain the formation of specifically morphological crystals. In this mechanism, primary particles self-assemble in preferential orientations into highly ordered superstructures with a well-defined external morphology.

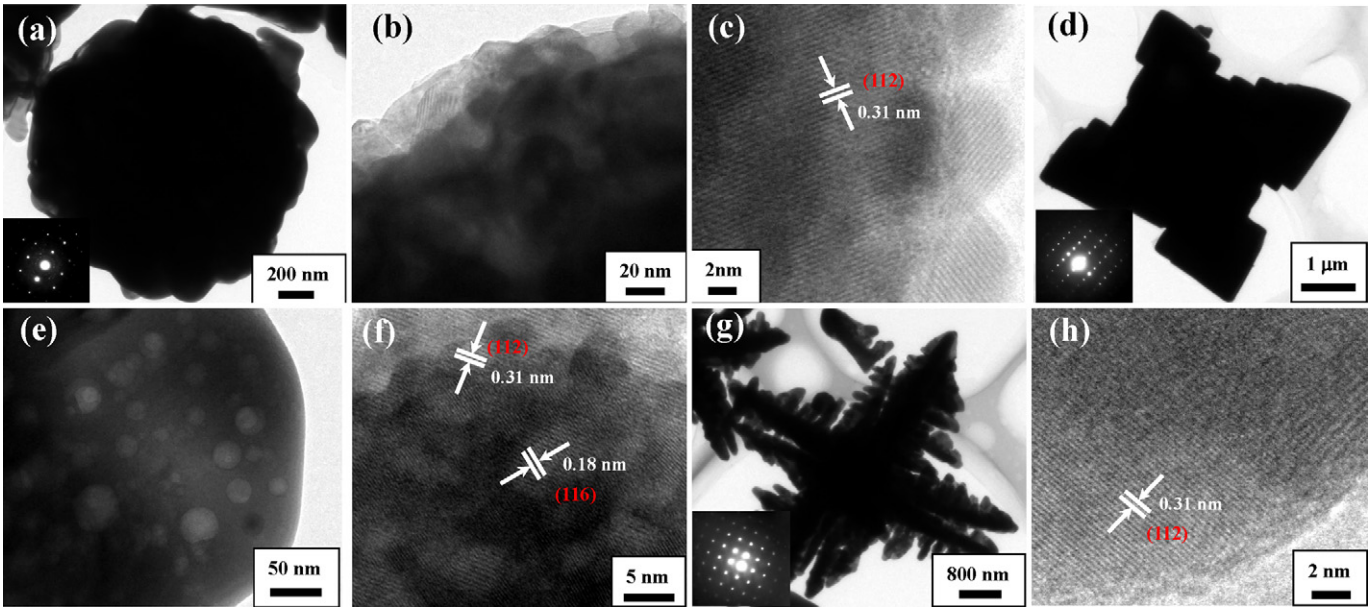

Fig. 3. TEM and high-resolution TEM images and SAED patterns (insets) of (a–c) $BiVO_4$–II, (d–f) $BiVO_4$–III, and (g, h) $BiVO_4$–V.

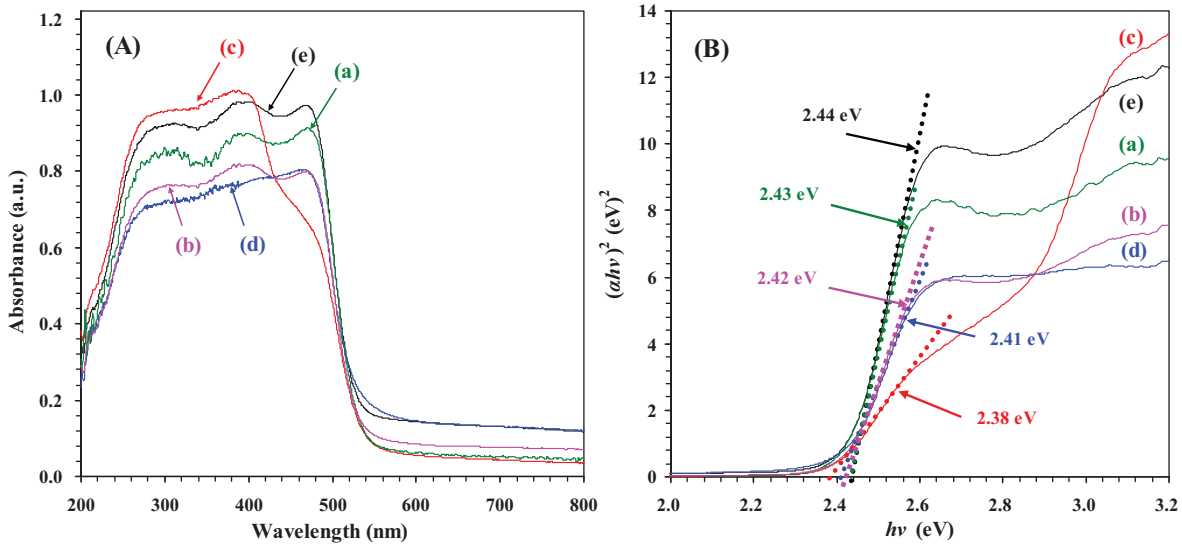

Fig. 4. (A) UV–Vis diffuse reflectance spectra and (B) plots of the $(\alpha h\nu)^2$ versus $h\nu$ of the $BiVO_4$–x samples with x = I (a), II (b), III (c), IV (d), and V (e).

Fig. S4 (Supplementary data) illustrates the formation mechanisms of the $BiVO_4$ materials with various morphologies under different conditions. In the case of surfactant-free synthesis, amorphous $BiVO_4$ nanoparticles were first produced at the initial stage, these primary nanoparticles then aggregated and self-assembled according to the specific orientation at a pH value of 3, and finally crystallized into hyperbranched $BiVO_4$ particles through an Ostwald ripening process and after calcination at 400 °C. In the case of P123-mediated synthesis, however, part of the surfactant molecules adsorbed on the surface of the $BiVO_4$ nuclei to decrease the surface energy of the nanocrystals [27,45–47]. The adsorption of P123 on the facets of nuclei might be inhomogeneous but selective [43]. Such a selective attachment of P123 and the oriented self-assembly of the P123-adsorbed nanoparticles were highly related to the external conditions, such as pH value of the precursor solution and hydrothermal temperature. The adsorbed P123 could work as a capping agent to decrease the growth rate of the adsorbed crystal faces and induce the compression along the axis perpendicular to these facets, thus forming two-dimensional (2D) $BiVO_4$ nanosheets or thin plate-like entities. Under different hydrothermal conditions (pH 3 or 6; alkaline source = $NH_3 \cdot H_2O$ or $NaHCO_3$; hydrothermal temperature = 80, 100 or 180 °C), the simultaneous collective self-assembly of these 2D nanoentities after the Ostwald ripening process and calcination at 400 °C for 4 h gave rise to $BiVO_4$ single-crystallites with a polyhedral, porous octapod-like or porous spherical morphology.

3.3. Light absorption property

Fig. 4(A) shows the UV–Vis diffuse reflectance spectra of the $BiVO_4$ samples. Although there were discrepancies in absorbance and absorption edge of the five $BiVO_4$ samples, they exhibited strong absorptions both in UV- and visible-light regions. Such featured absorption profiles suggest the generation of monoclinically crystallized $BiVO_4$ phases in the five $BiVO_4$ samples, as substantiated by the results of XRD and laser Raman studies. The steep shape of each spectrum indicates that the visible-light absorption was due to the band gap transition [48]. Band gap energy (E_g) can be used to evaluate the optical absorption performance of $BiVO_4$. Based on the equation of $(\alpha h\nu)^2 = A(h\nu - E_g)^n$ (where the A, α, and $h\nu$ represent constant, absorption coefficient, and incident photon energy, respectively) and the n value (=1 for direct transition [14]), one can estimate the E_g value from a plot of $(\alpha h\nu)^2$ versus photon energy ($h\nu$), as shown in Fig. 4(B). The intercept of the tangent to the X-axis is approximately equal to the E_g value [14,49–51]. The estimated E_g values of the $BiVO_4$ samples were listed in Table 1. Apparently, the E_g values of these monoclinic $BiVO_4$ samples with multiple morphologies fell into the range of 2.38–2.44 eV, slightly lower than or similar to those of $BiVO_4$ materials reported in the literature [3,4,6,11,14,15,37]. Compared to the $BiVO_4$ sample with a hyperbranched morphology, the porous octapod-like $BiVO_4$–III counterpart possessed a much lower band gap energy (2.38 eV). The result indicates that the $BiVO_4$–III sample was much more effective in absorbing visible light, and would hence show better photocatalytic activity for the degradation of organic dyes under visible-light illumination.

3.4. Photocatalytic performance

Shown in Fig. 5 is the photocatalytic performance of the $BiVO_4$ samples for the degradation of MB in an aqueous solution under visible-light illumination. For comparison purposes, we also conducted the experiments of MB direct photolysis (blank experiment) and MB degradation over the commercial TiO_2 nanoparticles (Degussa P25) under identical conditions. Apparently, MB could

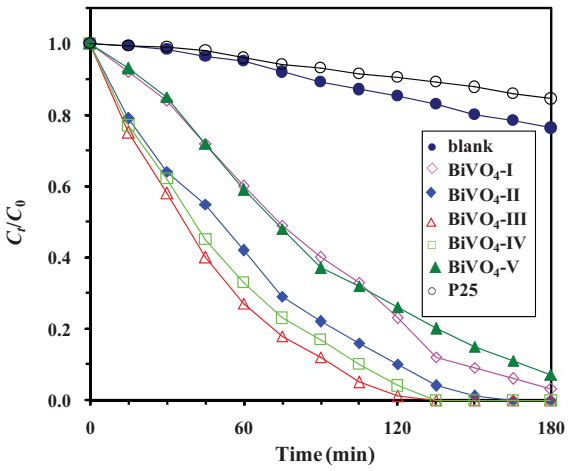

Fig. 5. Photocatalytic activities of the blank (direct photolysis), Degussa P25, and $BiVO_4$–x (x = I, II, III, IV and V) samples for the degradation of MB under visible-light ($\lambda \geq 400$ nm) irradiation.

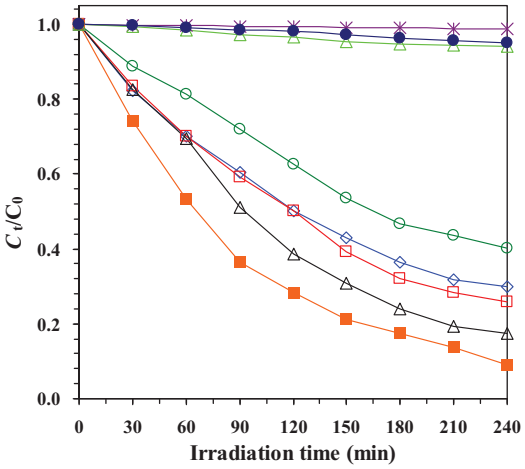

Fig. 6. Phenol concentration versus visible-light irradiation time: (✳) direct photolysis in the presence of H_2O_2, (●) Degussa P25 in the presence of H_2O_2, (△) $BiVO_4$–III in the absence of H_2O_2, and (◇) $BiVO_4$–I, (□) $BiVO_4$–II, (■) $BiVO_4$–III, (△) $BiVO_4$–IV, and (○) $BiVO_4$–V in the presence of H_2O_2 for the degradation of phenol (C_0 = 0.2 mmol/L) aqueous solution under visible-light (λ ≥ 400 nm) irradiation. (For interpretation of the references to colour in this figure legend, the reader is referred to the web version of the article.)

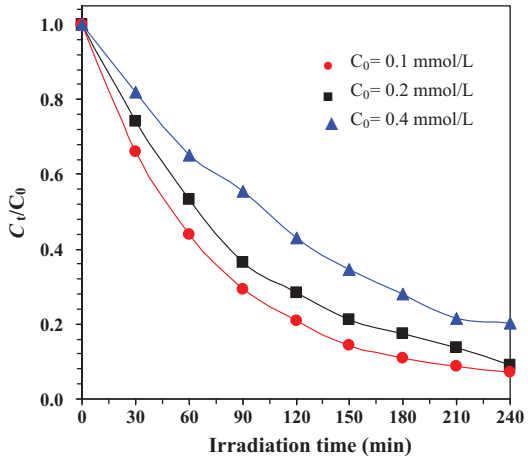

Fig. 7. Effect of the initial phenol concentration (C_0) on the photocatalytic performance of the $BiVO_4$–III sample for the degradation of phenol in the presence of the same amount of H_2O_2 under visible-light (λ ≥ 400 nm) irradiation.

be photolyzed under visible-light irradiation and 23% of MB was degraded within 3 h of reaction; the degradation efficiency of direct photolysis was higher than that achieved over the P25 photocatalyst. This result is understandable because P25 could not be photoexcited under visible-light irradiation and inhibited the direct photolysis of MB by shielding parts of the incident light [7]. The $BiVO_4$ samples showed much better visible-light-driven photocatalytic activities than the P25 sample. Among the five $BiVO_4$ samples, $BiVO_4$–II, $BiVO_4$–III, and $BiVO_4$–IV outperformed $BiVO_4$–I and $BiVO_4$–V, with the porous octapod-like $BiVO_4$–III and $BiVO_4$–IV samples exhibiting the best visible-light-driven photocatalytic activities: near 100% degradation of MB was achieved within 2 h of reaction. Such photocatalytic performance was much better than that (30–90% within 2 h of reaction) obtained over the $BiVO_4$ catalysts reported by other researchers [7,33,35,36,52]. It has been reported that the introduction of electron scavenger H_2O_2 could enhance the degradation rate of MB under the visible-light irradiation. For example, Das et al. [53] observed that the photodecolorization rate of MB over the TiP/TiO_2 or ZrP/TiO_2 catalyst increased after the addition of H_2O_2 under solar irradiation; Xiao et al. [54] claimed that the degradation efficiency of MB over the Co_3O_4/Bi_2WO_6 composite catalyst enhanced greatly in the presence of H_2O_2 under the visible-light irradiation. These authors thought that H_2O_2 addition decreased the recombination of the photoinduced hole–electron pairs.

Fig. 6 shows the photocatalytic activities of the as-prepared $BiVO_4$ and P25 samples for the degradation of phenol in aqueous solution in the absence and presence of a small amount of H_2O_2 under visible-light illumination. It is clearly observed that after visible-light irradiation for 4 h, the phenol conversion was only ca. 4% over the P25 sample, whereas it almost unchanged in the direct photolysis of phenol in the presence of H_2O_2, indicating that the photolysis of phenol was negligible under the present condition, in agreement with the results reported by other researchers [22,23]. The drop of phenol concentration in the degradation of phenol over the $BiVO_4$–III sample in the absence of H_2O_2 under visible-light irradiation was quite small (only ca. 6% of phenol conversion was achieved after 4 h of reaction), which was due to the poor adsorption of phenol in the aqueous solution over the $BiVO_4$ catalyst [55] and the weak ability of oxygen to capture the photogenerated electrons [23]. The $BiVO_4$ samples in the presence of H_2O_2, however, showed excellent visible-light-driven catalytic performance. This result demonstrates the presence of a synergistic effect between the photocatalyst and the electron scavenger. As an efficient electron scavenger, H_2O_2 could trap the photoinduced electrons and effectively inhibited the recombination of electron–hole pairs [55]. It can be realized from Fig. 6 that the photocatalytic activities over the as-prepared $BiVO_4$ catalysts within 4 h of reaction decreased according to the sequence of $BiVO_4$–III (ca. 91%) > $BiVO_4$–IV (ca. 83%) > $BiVO_4$–II (ca. 74%) > $BiVO_4$–I (ca. 70%) > $BiVO_4$–V (ca. 60%). Obviously, the porous octapod-like $BiVO_4$–III photocatalyst performed much better than the nonoporous hyperbranched $BiVO_4$–V photocatalyst. It is worth pointing out that no detectable reaction intermediates were generated over our $BiVO_4$ samples during the photocatalytic processes under visible-light irradiation. For example, in addition to the adsorption peak at ca. 280 nm, no other absorption peaks assignable to the intermediates appeared in the UV–Vis absorption spectra of the solutions after phenol photodegradation at different times over the $BiVO_4$–III catalyst (Fig. S5 of the Supplementary data). In other words, phenol was photocatalytically degraded to CO_2 and H_2O over the $BiVO_4$ samples under visible-light illumination. Therefore, the photocatalytic activity data estimated from the variations of absorbance of phenol in the solution were reliable. Such an activity measurement was also been adopted by Wang and coworkers [25]. Fig. 7 shows the effect of phenol concentration on the photocatalytic activity of the $BiVO_4$–III sample for phenol degradation in the presence of H_2O_2 under visible-light irradiation. It is seen that within 4 h of visible-light irradiation, a higher phenol conversion could be achieved over this sample for the solution with a lower phenol concentration. Such a phenomenon was also observed in the photocatalytic degradation of phenol [56] and MB [57] over the TiO_2-based catalysts.

It has been generally accepted that the crystallite size, crystal structure, crystallinity, morphology, and surface area of a material are important factors influencing its photocatalytic performance [6,58,59]. By comparing the photocatalytic performance of the as-prepared $BiVO_4$ samples, one can realize that there was no obvious relation of the crystallite or particle size with the catalytic activity. The XRD results reveal that all of the as-prepared $BiVO_4$ samples were monoclinic and similar in crystallinity, meaning that the crystal structure and crystallinity would not lead to the big discrepancy in photocatalytic performance of these samples. In other words, other factors, such as surface area, morphology, pore structure, and band gap energy might determine the photocatalytic activity of bismuth vanadate. Among the as-prepared $BiVO_4$ samples, the $BiVO_4$–III sample with a porous octapod-like morphology had

a much higher surface area (11.8 m^2/g) and a much lower band gap energy (2.38 eV) than the nonporous hyperbranched $BiVO_4$–V sample (Table 1). Furthermore, the presence of porous structure could favor the adsorption and diffusion of reactants as well as the facile accessibility of incident light to more surfaces of the catalyst [60], thus giving rise to the improvement in photocatalytic performance of $BiVO_4$–III.

Base on the above characterization results and activity data, we conclude that the excellent visible-light-driven catalytic performance of the porous monoclinic $BiVO_4$–III sample was related to its high surface area, good pore structure, unique particle morphology, and low band gap energy.

4. Conclusions

By adopting the hydrothermal strategy with bismuth nitrate and ammonium metavanadate as metal source at pH 3 or 6, $NH_3{\cdot}H_2O$ or $NaHCO_3$ as pH regulator, and after calcination at 400 °C for 6 h, one could generate monoclinic $BiVO_4$ single-crystallites with hyperbranched, polyhedral, porous spherical or porous octapod-like morphologies in the absence or presence of P123. It is found that the particle morphology of the final product $BiVO_4$ was strongly dependent on the factors, such as the pH value of the precursor solution, surfactant, and hydrothermal temperature. The introduction of P123 to the precursor solution promoted the fabrication of $BiVO_4$ with a porous structure. The surfactant P123 played an important role in the selective preparation of specifically architectural $BiVO_4$. Among the five $BiVO_4$ samples, the $BiVO_4$–II, $BiVO_4$–III, and $BiVO_4$–IV ones generated hydrothermally with P123 exhibited good optical absorption behaviors both in UV- and visible-light regions and thus showed excellent photocatalytic performance for the removal of phenol and MB under visible-light illumination. It is concluded that high surface area, porous structure, unique particle morphology, and low band gap energy account for the excellent visible-light-driven catalytic performance of the porous spherical or porous octapod-like $BiVO_4$ single-crystallites with a monoclinic crystal structure.

Acknowledgements

The work described was supported by the Creative Research Foundation of Beijing University of Technology (00500054R4003 and 005000543111501), "863" Key Program of Ministry of Science and Technology of China (2009AA063201), the NSF of China (20973017 and 21077007), and the Funding Project for Academic Human Resources Development in Institutions of Higher Learning under the Jurisdiction of Beijing Municipality (PHR201007105 and PHR201107104). We also thank Mrs. Jianping He (State Key Laboratory of Advanced Metals and Materials, University of Science & Technology Beijing) for doing the SEM analysis of the samples.

Appendix A. Supplementary data

Supplementary data associated with this article can be found, in the online version, at doi:10.1016/j.jhazmat.2012.02.073.

References

[1] W.I.F. David, I.G. Wood, Ferroelastic phase-transitions in $BiVO_4$: VI. Some comments on the relationship between spontaneous deformation and domain-walls in ferroelastics, J. Phys. C: Solid State Phys. 16 (1983) 5149–5166.
[2] D. Barreca, L.E. Depero, V. Di Noto, G.A. Rizzi, L. Sangaletti, E. Tondello, Thin films of bismuth vanadates with modifiable conduction properties, Chem. Mater. 11 (1999) 255–261.
[3] S. Tokunaga, H. Kato, A. Kudo, Selective preparation of monoclinic and tetragonal $BiVO_4$ with scheelite structure and their photocatalytic properties, Chem. Mater. 13 (2001) 4624–4628.
[4] A. Kudo, K. Omori, H. Kato, A novel aqueous process for preparation of crystal form-controlled and highly crystalline $BiVO_4$ powder from layered vanadates at room temperature and its photocatalytic and photophysical properties, J. Am. Chem. Soc. 121 (1999) 11459–11467.
[5] A.W. Sleight, H.-Y. Chen, A. Ferretti, D.E. Cox, Crystal-growth and structure of $BiVO_4$, Mater. Res. Bull. 14 (1979) 1571–1581.
[6] J.Q. Yu, A. Kudo, Effects of structural variation on the photocatalytic performance of hydrothermally synthesized $BiVO_4$, Adv. Funct. Mater. 16 (2006) 2163–2169.
[7] X. Zhang, Z.H. Ai, F.L. Jia, L.Z. Zhang, X.X. Fan, Z.G. Zou, Selective synthesis and visible-light photocatalytic activities of $BiVO_4$ with different crystalline phases, Mater. Chem. Phys. 103 (2007) 162–167.
[8] J.Q. Yu, A. Kudo, Hydrothermal synthesis of nanofibrous bismuth vanadate, Chem. Lett. 34 (2005) 850–851.
[9] J.B. Liu, H. Wang, S. Wang, H. Yan, Hydrothermal preparation of $BiVO_4$ powders, Mater. Sci. Eng. B 104 (2003) 36–39.
[10] L. Zhang, D.R. Chen, X.L. Jiao, Monoclinic structured $BiVO_4$ nanosheets: hydrothermal preparation, formation mechanism, and coloristic and photocatalytic properties, J. Phys. Chem. B 110 (2006) 2668–2673.
[11] H.B. Li, G.C. Liu, X.C. Duan, Monoclinic $BiVO_4$ with regular morphologies: hydrothermal synthesis, characterization and photocatalytic properties, Mater. Chem. Phys. 115 (2009) 9–13.
[12] K. Sayama, A. Nomura, Z.G. Zou, R. Abe, Y. Abe, H. Arakawa, Photoelectrochemical decomposition of water on nanocrystalline $BiVO_4$ film electrodes under visible light, Chem. Commun. (2003) 2908–2909.
[13] A. Galembeck, O.L. Alves, $BiVO_4$ thin film preparation by metalorganic decomposition, Thin Solid Films 365 (2000) 90–93.
[14] L. Zhou, W.Z. Wang, S.W. Liu, L.S. Zhang, H.L. Xu, W. Zhu, A sonochemical route to visible-light-driven high-activity $BiVO_4$ photocatalyst, J. Mol. Catal. A 252 (2006) 120–124.
[15] Y. Zhao, Y. Xie, X. Zhu, S. Yan, S.X. Wang, Surfactant-free synthesis of hyperbranched monoclinic bismuth vanadate and its applications in photocatalysis, gas sensing, and lithium-ion batteries, Chem. Eur. J. 14 (2008) 1601–1606.
[16] L. Zhou, W.Z. Wang, L.S. Zhang, H.L. Xu, W. Zhu, Single-crystalline $BiVO_4$ microtubes with square cross-sections: microstructure, growth mechanism, and photocatalytic property, J. Phys. Chem. C 111 (2007) 13659–13664.
[17] A.P. Zhang, J.Z. Zhang, Characterization of visible-light-driven $BiVO_4$ photocatalysts synthesized via a surfactant-assisted hydrothermal method, Spectrochim. Acta A 73 (2009) 336–341.
[18] G.S. Li, D.Q. Zhang, J.C. Yu, Ordered mesoporous $BiVO_4$ through nanocasting: a superior visible light-driven photocatalyst, Chem. Mater. 20 (2008) 3983–3992.
[19] Y. Zhou, K. Vuille, A. Heel, B. Probst, R. Kontic, G.R. Patzke, An inorganic hydrothermal route to photocatalytically active bismuth vanadate, Appl. Catal. A 375 (2010) 140–148.
[20] A. Zaleska, E. Grabowska, J.W. Sobczak, M. Gazda, J. Hupka, Photocatalytic activity of boron-modified TiO_2 under visible light: the effect of boron content, calcination temperature and TiO_2 matrix, Appl. Catal. B 89 (2009) 469–475.
[21] Z.J. Zhang, W.Z. Wang, W.Z. Yin, M. Shang, L. Wang, S.M. Sun, Inducing photocatalysis by visible light beyond the absorption edge: effect of upconversion agent on the photocatalytic activity of Bi_2WO_6, Appl. Catal. B 101 (2010) 68–73.
[22] W.Z. Yin, W.Z. Wang, S.M. Sun, Photocatalytic degradation of phenol over cage-like Bi_2MoO_6 hollow spheres under visible-light irradiation, Catal. Commun. 11 (2010) 647–650.
[23] B.P. Xie, H.X. Zhang, P.X. Cai, R.L. Qiu, Y. Xiong, Simultaneous photocatalytic reduction of Cr(VI) and oxidation of phenol over monoclinic $BiVO_4$ under visible light irradiation, Chemosphere 63 (2006) 956–963.
[24] N.C. Castillo, L. Ding, A. Heel, T. Graule, C. Pulgarin, On the photocatalytic degradation of phenol and dichloroacetate by $BiVO_4$: the need of a sacrificial electron acceptor, J. Photochem. Photobiol. A 216 (2010) 221–227.
[25] Z.J. Zhang, W.Z. Wang, M. Shang, W.Z. Yin, Photocatalytic degradation of rhodamine B and phenol by solution combustion synthesized $BiVO_4$ photocatalyst, Catal. Commun. 11 (2010) 982–986.
[26] G.Z. Wang, L. Zhang, H.X. Dai, J.G. Deng, C.X. Liu, H. He, C.T. Au, P123-assisted hydrothermal synthesis and characterization of rectangular parallelepiped and hexagonal prism single-crystalline MgO with three-dimensional wormholelike mesopores, Inorg. Chem. 47 (2008) 4015–4022.
[27] C.X. Liu, L. Zhang, J.G. Deng, Q. Mu, H.X. Dai, H. He, Surfactant-aided hydrothermal synthesis and carbon dioxide adsorption behavior of three-dimensionally mesoporous calcium oxide single-crystallites with tri-, tetra-, and hexagonal morphologies, J. Phys. Chem. C 112 (2008) 19248–19256.
[28] H.N. Li, L. Zhang, H.X. Dai, H. He, Facile synthesis and unique physicochemical properties of three-dimensionally ordered macroporous magnesium oxide, gamma-alumina, and ceria-zirconia solid solutions with crystalline mesoporous walls, Inorg. Chem. 48 (2009) 4421–4434.
[29] X. Meng, L. Zhang, H.X. Dai, Z.X. Zhao, R.Z. Zhang, Y.X. Liu, Surfactant-assisted hydrothermal fabrication and visible-light-driven photocatalytic degradation of methylene blue over multiple morphological $BiVO_4$ single-crystallites, Mater. Chem. Phys. 125 (2011) 59–65.
[30] H.Y. Jiang, H.X. Dai, X. Meng, L. Zhang, J.G. Deng, K.M. Ji, Morphology-dependent photocatalytic performance of monoclinic $BiVO_4$ for methyl orange degradation under visible-light irradiation, Chin. J. Catal. 32 (2011) 939–949.
[31] H.Y. Jiang, H.X. Dai, X. Meng, L. Zhang, J.G. Deng, K.M. Ji, Porous olive-like $BiVO_4$: alcoho-hydrothermal preparation and excellent visible-light-driven photocatalytic performance for the degradation of phenol, Appl. Catal. B 105 (2011) 326–334.

[32] L. Zhou, W.Z. Wang, H.L. Xu, Controllable synthesis of three-dimensional well-defined $BiVO_4$ mesocrystals via a facile additive-free aqueous strategy, Cryst. Growth Des. 8 (2008) 728–733.
[33] J.Q. Yu, Y. Zhang, A. Kudo, Synthesis and photocatalytic performances of $BiVO_4$ by ammonia co-precipitation process, J. Solid State Chem. 182 (2009) 223–228.
[34] M. Gotić, S. Musić, M. Ivanda, M. Šoufek, S. Popović, Synthesis and characterisation of bismuth(III) vanadate, J. Mol. Struct. 744–747 (2005) 535–540.
[35] H.Q. Jiang, M. Nagai, K. Kobayashi, Enhanced photocatalytic activity for degradation of methylene blue over $V_2O_5/BiVO_4$ composite, J. Alloys Compd. 479 (2009) 821–827.
[36] H. Xu, H.M. Li, C.D. Wu, J.Y. Chu, Y.S. Yan, H.M. Shu, Z. Gu, Preparation, characterization and photocatalytic properties of Cu-loaded $BiVO_4$, J. Hazard. Mater. 153 (2008) 877–884.
[37] L.Z. Li, B. Yan, $BiVO_4/Bi_2O_3$ submicrometer sphere composite: microstructure and photocatalytic activity under visible-light irradiation, J. Alloys Compd. 476 (2009) 624–628.
[38] A.P. Zhang, J.Z. Zhang, N.Y. Cui, X.Y. Tie, Y.W. An, L.J. Li, Effects of pH on hydrothermal synthesis and characterization of visible-light-driven $BiVO_4$ photocatalyst, J. Mol. Catal. A 304 (2009) 28–32.
[39] A.W. Xu, M. Antonietti, H. Cölfen, Y.P. Fang, Uniform hexagonal plates of vaterite $CaCO_3$ mesocrystals formed by biomimetic mineralization, Adv. Funct. Mater. 16 (2006) 903–908.
[40] O. Grassmann, P. Löbmann, Morphogenetic control of calcite crystal growth in sulfonic acid based hydrogels, Chem. Eur. J. 9 (2003) 1310–1316.
[41] S.H. Yu, H. Cölfen, Bio-inspired crystal morphogenesis by hydrophilic polymers, J. Mater. Chem. 14 (2004) 2124–2147.
[42] T.P. Wang, M. Antonietti, H. Colfen, Calcite mesocrystals: morphing crystals by a polyelectrolyte, Chem. Eur. J. 12 (2006) 5722–5730.
[43] Q. Gong, X.F. Qian, X.D. Ma, Z.K. Zhu, Large-scale fabrication of novel hierarchical 3D $CaMoO_4$ and $SrMoO_4$ mesocrystals via a microemulsion-mediated route, Cryst. Growth Des. 6 (2006) 1821–1825.
[44] X.H. Guo, S.H. Yu, Controlled mineralization of barium carbonate mesocrystals in a mixed solvent and at the air/solution interface using a double hydrophilic block copolymer as a crystal modifier, Cryst. Growth Des. 7 (2007) 354–359.
[45] Y.-W. Jun, J.-S. Choi, J. Cheon, Shape control of semiconductor and metal oxide nanocrystals through nonhydrolytic colloidal routes, Angew. Chem. Int. Ed. 45 (2006) 3414–3439.
[46] C. Burda, X.B. Chen, R. Narayanan, M.A. EI-Sayed, Chemistry and properties of nanocrystals of different shapes, Chem. Rev. 105 (2005) 1025–1102.
[47] Y.J. Zhang, L. Zhang, J.G. Deng, H.X. Dai, H. He, Controlled synthesis, characterization, and morphology-dependent reducibility of ceria-zirconia-yttria solid solutions with nanorod-like, microspherical, microbowknot-like, and micro-octahedral shapes, Inorg. Chem. 48 (2009) 2181–2192.
[48] C. Zhang, Y.F. Zhu, Synthesis of square Bi_2WO_6 nanoplates as high-activity visible-light-driven photocatalysts, Chem. Mater. 17 (2005) 3537–3545.
[49] M.A. Butler, Photoelectrolysis and physical-properties of semiconducting electrode WO_3, J. Appl. Phys. 48 (1977) 1914–1920.
[50] J.C. Yu, J.G. Yu, W.K. Ho, Z.T. Jiang, L.Z. Zhang, Effects of F-doping on the photocatalytic activity and microstructures of nanocrystalline TiO_2 powders, Chem. Mater. 14 (2002) 3808–3816.
[51] J.G. Yu, J.C. Yu, W.K. Ho, Z.T. Jiang, Effects of calcination temperature on the photocatalytic activity and photo-induced super-hydrophilicity of mesoporous TiO_2 thin films, New J. Chem. 26 (2002) 607–613.
[52] W.F. Yao, H. Iwai, J.H. Ye, Effects of molybdenum substitution on the photocatalytic behavior of $BiVO_4$, Dalton Trans. (2008) 1426–1430.
[53] D.P. Das, N. Baliarsingh, K.M. Parida, Photocatalytic decolorisation of methylene blue (MB) over titania pillared zirconium phosphate (ZrP) and titanium phosphate (TiP) under solar radiation, J. Mol. Catal. A 261 (2007) 254–261.
[54] Q. Xiao, J. Zhang, C. Xiao, X.K. Tan, Photocatalytic degradation of methylene blue over Co_3O_4/Bi_2WO_6 composite under visible light irradiation, Catal. Commun. 9 (2008) 1247–1253.
[55] M. Shang, W.Z. Wang, S.M. Sun, J. Ren, L. Zhou, L. Zhang, Efficient visible light-induced photocatalytic degradation of contaminant by spindle-like $PANI/BiVO_4$, J. Phys. Chem. C 113 (2009) 20228–20233.
[56] C.H. Chiou, C.Y. Wu, R.S. Juang, Influence of operating parameters on photocatalytic degradation of phenol in UV/TiO_2 process, Chem. Eng. J. 139 (2008) 322–329.
[57] S. Senthilkumaar, K. Porkodi, R. Vidyalakshmi, Photodegradation of a textile dye catalyzed by sol-gel derived nanocrystalline TiO_2 via ultrasonic irradiation, J. Photochem. Photobiol. A 170 (2005) 225–232.
[58] D.L. Liao, B.Q. Liao, Shape, size and photocatalytic activity control of TiO_2 nanoparticles with surfactants, J. Photochem. Photobiol. A 187 (2007) 363–369.
[59] J.S. Valente, F. Tzompantzi, J. Prince, J.G.H. Cortez, R. Gomez, Adsorption and photocatalytic degradation of phenol and 2,4 dichlorophenoxiacetic acid by Mg–Zn–Al layered double hydroxides, Appl. Catal. B 90 (2009) 330–338.
[60] M. Sun, D.Z. Li, W.J. Zhang, Z.X. Chen, H.J. Huang, W.J. Li, Y.H. He, X.Z. Fu, Photocatalyst $Cd_2Sb_2O_{6.8}$ with high photocatalytic activity toward benzene and dyes, J. Phys. Chem. C 113 (2009) 14916–14921.